

# Solvent Dependence of Absorption and Emission Spectra of Ru(bpy)<sub>2</sub>(CN)<sub>2</sub>: Experiment and Explanation Based on Electronic Structure Theory

Lajos Fodor,<sup>†</sup> György Lendvai,<sup>†,‡,\*</sup> and Attila Horváth<sup>†</sup>

Department of General and Inorganic Chemistry, Institute of Chemistry, University of Pannonia, H-8201 Veszprém, P.O. Box 158, Hungary, Institute of Structural Chemistry, Chemical Research Center, Hungarian Academy of Sciences, H-1525 Budapest, P.O. Box 17, Hungary

Received: July 17, 2007; In Final Form: September 4, 2007

Measurements in acidic media and time-dependent density functional theory and  $\Delta$ SCF calculations were performed for Ru(bpy)<sub>2</sub>(CN)<sub>2</sub> in 11 solvents of varying polarity to determine the solvent's influence on the absorption and emission spectra of the complex. The solvent effect caused by both the polarizable continuum nature of the solvent (characterized by the polarizable conductor model), and by the coordination of the cyano groups of the complex by solvent molecules were investigated. Both the absorption and emission maxima show a strong blue shift as the solute–solvent interaction increases, the magnitude of which is in good linear correlation with Gutmann's acceptor number of the solvent. The calculations reproduce the location, shape, and shift of the experimental metal-to-ligand charge transfer bands. The solvent shift is shown to be in good correlation with the charge difference between the Ru atom and the bpy ligand, which in turn is closely related to the HOMO energy. The coordination of the solvent molecule to the cyano group causes a smaller blue shift than the polarizable continuum solvent. The specific solute–solvent interaction becomes dominant, however, when the pH in a protic solvent is small and the complex is protonated.

## Introduction

The complexes of Ru(II) formed with  $\alpha,\alpha'$ -diimine ligands, such as [Ru(bpy)<sub>3</sub>]<sup>2+</sup> and [Ru(phen)<sub>3</sub>]<sup>2+</sup> (bpy = 2,2'-bipyridine and phen = 1,10-phenanthroline), are widely used as photosensitizers in various photochemical systems because of their excellent photophysical and photochemical characteristics. Considerable attention has also been devoted to RuL<sub>2</sub>X<sub>2</sub> complexes (where L is an  $\alpha,\alpha'$ -diimine ligand, such as bpy, phen, and their derivatives; X = halide or pseudohalide ligand, such as Cl<sup>-</sup>, CN<sup>-</sup>, SCN<sup>-</sup>) due to their ground- and excited-state properties potential for solar energy conversion<sup>1–4</sup> and their applicability as building blocks of supramolecular devices capable of performing useful light-induced functions.<sup>5–7</sup> Although [Ru(bpy)<sub>2</sub>(CN)<sub>2</sub>] has been proved to be one of the best species for these purposes, the structure of this complex has not been determined by single-crystal X-ray technique: only a few studies based on quantum chemical calculations have been performed to obtain its molecular geometry and to analyze the electronic structure background of the spectroscopically observed significant solute–solvent interactions. As has been pointed out, these interactions can be used to tune the dye-sensitized nanocrystalline solar cell<sup>8,9</sup> or the luminescence properties of a bichromophoric supramolecule.<sup>10</sup> Recently, it has also been demonstrated that the proton-driven, self-assembled, nanoscale molecular structures based on mixed ligand ruthenium(II) cyanocomplexes is an efficient antenna system for light harvesting and its conversion to chemical energy.<sup>11</sup>

To optimize the performance of a sensitizer or the light-harvesting characteristics, it is important to know the optical

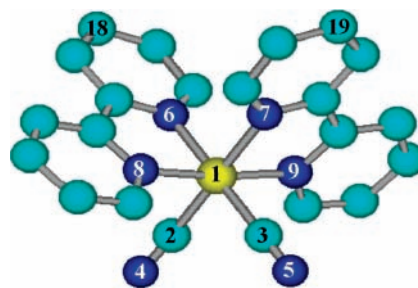


Figure 1. The structure of Ru(bpy)<sub>2</sub>(CN)<sub>2</sub> and numbering of the atoms.

absorption and emission spectra of the complex. In addition to experiments, theory has recently become an efficient tool in determining such properties. Electronic structure theory achieved the level when prediction of the location of absorption and emission maxima is possible with relatively small and generally systematic error. In addition, the solvent dependence of these properties can also be determined. The most generally applicable method for this purpose is the time-dependent density functional theory (TD-DFT).<sup>12–15</sup>

The purpose of this work is to understand the factors determining the absorption and emission spectrum and its solvent shift for a prototype sensitizer, Ru(bpy)<sub>2</sub>(CN)<sub>2</sub>, using electronic structure theory. Both experiments and TD-DFT calculations have been performed for the complex in various solvents to test the methods of electronic structure theory as well as to explore the change of the electron distribution of the complex as the solvent is systematically changed and its connection to the electronic spectrum. The comparison of theory and experiment provides a basis for testing the quality of the electronic structure method we applied. Because electronic structure calculations are approximate, their accuracy needs to

\* Corresponding author. Tel.: +36 1 4384124. Fax: +36 1 3257554. E-mail: lendvai@chemres.hu.

<sup>†</sup> University of Pannonia.

<sup>‡</sup> Hungarian Academy of Sciences.

**TABLE 1: Selected Bond Lengths (Å) and Angles (deg) of the Singlet (<sup>1</sup>A) and Triplet (<sup>3</sup>A and <sup>3</sup>B) States of Ru(bpy)<sub>2</sub>(CN)<sub>2</sub> Complex Calculated in This Work and of Ru(bpy)<sub>2</sub>(CNx)<sub>2</sub> and Ru(bpy)<sub>2</sub>(NCS)<sub>2</sub> Based on X-ray Crystallography from Refs 22 and 37, Respectively**

distances, angles	S <sub>0</sub> ( <sup>1</sup> A)	Ru(bpy) <sub>2</sub> (CNx) <sub>2</sub> <sup>a</sup>	Ru(bpy) <sub>2</sub> (NCS) <sub>2</sub>	T <sub>1</sub> ( <sup>3</sup> B)	T <sub>1</sub> ( <sup>3</sup> A)
Ru–N(6)	2.124	2.109	2.041	2.130	2.130
Ru–N(8)	2.076	2.079	2.051	2.090	2.097
Ru–C(2)	2.022	1.949	2.055 (Ru–N)	2.017	2.016
C(2)–N(4)	1.193	1.165	1.124	1.193	1.193
N(6)–Ru–N(8)	78.0	78.3	78.7	78.5	78.3
C(2)–Ru–C(3)	91.4	90.7	88.7 (NRuN)	93.0	94.8
Ru–C(2)–N(4)	175.3	177.2	168.2 (RuNC)	176.8	176.6
N(6)–Ru–N(7)	93.4	85.5	90.7	87.3	85.1
N(8)–Ru–N(9)	176.1	166.5	173.0	174.5	176.0
C(2)–Ru–N(7)	171.9			172.8	171.1
N(8)–Ru–N(7)	99.3	92.5	96.4	97.5	98.8
C(18)–C(19)	7.379			6.964	6.760

<sup>a</sup> CNx = 2,6-dimethylphenylisocyanide.

be tested against experiment in at least a few cases as calibration points. In this way, the reliability of their results can be made quantitative.

The spectral characteristics of our target complex, Ru(bpy)<sub>2</sub>(CN)<sub>2</sub>, have been widely studied and are a subject of extensive measurements in our laboratory.<sup>16</sup> Despite wide interest in this compound, no crystal structure data are available in the literature. The geometry of this complex has been calculated by density functional theory by Adamo and co-workers,<sup>17</sup> who used the PBE0<sup>18</sup> functional. They also calculated the electronic spectrum of Ru(bpy)<sub>2</sub>(CN)<sub>2</sub> using TD-DFT in vacuum and in water (for a description of the solvent effect, they used the conductor-like solvation model, COSMO or polarizable conductor model (CPCM) method<sup>19–21</sup>). More detailed information has been accumulated in the literature concerning TD-DFT calculation of absorption characteristics of some other Ru(II)-diimine complexes in solution.<sup>17,22–28</sup>

In the rest of this paper, after summarizing the experimental and theoretical methods, the results of the measured and calculated absorption and emission spectra are presented, and then the correlations observed between the spectral properties, the change of the electronic structure of the molecule with the characteristics of the solvents are discussed.

## Experimental

**Materials.** [Ru(bpy)<sub>2</sub>(CN)<sub>2</sub>]<sub>2</sub>·2H<sub>2</sub>O was prepared and purified by the method of Demas et al.<sup>29</sup> Its purity was checked by IR, <sup>1</sup>H NMR and UV–vis absorption and emission spectroscopy. Water purified by a Millipore Super-Q system was used to prepare aqueous solutions. Methanol, acetonitrile, dichloromethane, and chloroform (analytical grade) were purchased from Sigma-Aldrich or Reanal and used without further purification.

**Instruments.** UV–vis absorption spectra were obtained using a Specord S100 diode array spectrophotometer. Luminescence emission spectra were measured by a Perkin-Elmer LS50B spectrofluorimeter.

**Computational Details.** The molecular geometry of the singlet ground state and the first excited triplet state have been calculated by DFT using the B3LYP<sup>30,31</sup> hybrid functional and the LANL2DZ basis set.<sup>32–34</sup> Both are proper minima (have no imaginary normal-mode frequency). Our extensive attempts to optimize the geometry of the complex in solvents failed due to the lack of convergence of the geometry optimization. The influence of the changes of the geometry on the spectral properties (by selecting a few from the fluctuating series of geometries) was tested and was found to be negligible (the absorption energy varied by less than 100 cm<sup>-1</sup>). The geometry

optimizations and the energies of the excited states were calculated by TD-DFT as implemented in Gaussian 03.<sup>15,35</sup> The energy corresponding to phosphorescence was determined by two approaches. One is the ΔSCF method, in which the emission energy was obtained as the difference between the energy obtained in separate SCF calculations for the triplet and singlet state at the geometry of the triplet minimum. The other method we used was TD-DFT, started from the singlet state at the triplet geometry. The influence of the solvent was approximated by the polarizable conductor model.<sup>19</sup> The specific interactions in protic solvents were modeled by calculating the structure and energy of the protonated complex and the adduct of [Ru(bpy)<sub>2</sub>(CN)<sub>2</sub>] with two H<sub>2</sub>O or CH<sub>3</sub>CN molecules. In the calculation of the absorption spectra, the 40 or 50 lowest spin-allowed singlet–singlet transitions were taken into account up to transition energies of at least 40 000 cm<sup>-1</sup>. The absorption spectra have been simulated in the following way: Each spectral line predicted by TD-DFT was “widened” into a Gaussian function characterized by σ = 1000–2300 cm<sup>-1</sup>, which corresponds to a full width at half-maximum (fwhm) of ~2350–5400 cm<sup>-1</sup> and a height that guaranteed that the area under the “spectral band” is the same as the TD-DFT oscillator strength.<sup>36</sup> The “absorption intensities” obtained this way at each transition wavenumber from all “bands” were summarized and plotted. In the discussion below, the location of the band maxima correspond to the maxima of the simulated spectrum. We selected this parameter to discuss the spectral shift with the polarity of the solvent because (1) in this way, the cumulative effect of several close-lying transitions appear together; and (2) the simulated spectra are more directly comparable with the experiment than the individual calculated “spectral lines”. For the analysis of the charge distribution in the complex, we used Mulliken population analysis. Similar conclusions could be drawn on the basis of other atomic charge definitions.

## Results and Discussion

**Molecular Geometry.** The molecular geometry in the gas phase in both the singlet and triplet state was optimized by confining the symmetry to the C<sub>2</sub> point group. Selected bond distances and angles are listed in Table 1, and the structure and the numbering of atoms is shown in Figure 1. Because our attempts to optimize the molecular geometry in solvents failed (this experience is similar to that of Villegas et al.<sup>22</sup> and De Angelis et al.<sup>24</sup>), we used the geometry obtained in the gas phase for all spectrum calculations.

The Ru(bpy)<sub>2</sub>(CN)<sub>2</sub> complex in the singlet ground state adopts a distorted octahedral geometry. In the lack of single-crystal X-ray structure for Ru(bpy)<sub>2</sub>(CN)<sub>2</sub>, the obtained geometrical

parameters were compared with those of two similar complexes for which X-ray data are available: Ru(bpy)<sub>2</sub>(NCS)<sub>2</sub><sup>37</sup> and Ru(bpy)<sub>2</sub>(CNx)<sub>2</sub> (where CNx = 2,6-dimethylphenylisocyanide)<sup>22</sup> (Table 1). The angles of the trans ligands at the metal center were 176.1° for N(bpy)–Ru–N(bpy') and 171.9° for N(bpy)–Ru–C. The Ru–N(bpy, trans to CN) bond length is longer by ~0.06 Å than the Ru–N(bpy, cis to CN) distance. This result is in good agreement with the experimental data for Ru(bpy)<sub>2</sub>(CNx)<sub>2</sub> and can be explained by the strong trans effect of the CN ligand, which makes the Ru–N(bpy, trans to CN) bonds weaker than Ru–N(bpy cis to CN). The Ru–CN and C–N(cyano) distance is similar to the bond length determined in a Na<sub>4</sub>[Ru(CN)<sub>6</sub>] single crystal<sup>38</sup> (2.02 and 1.16 Å, respectively) and measured for (PPN)<sub>2</sub>[Ru(bpy)(CN)<sub>4</sub>]·2MeCN·2Et<sub>2</sub>O·2H<sub>2</sub>O (PPN = bis(triphenylphosphine)iminium)<sup>39</sup> (1.99–2.07 and 1.12–1.16 Å, respectively) on the basis of single-crystal X-ray analysis. Although the N6(bpy)–Ru–N8(bpy) angle (78.0°) in Ru(bpy)<sub>2</sub>(CN)<sub>2</sub> is the same as in the Ru(bpy)<sub>2</sub>(CNx)<sub>2</sub> complex (78.3°), the N8(bpy)–Ru–N7(bpy') and N8(bpy)–Ru–N9(bpy') angles are much wider in the cyano than in the CNx complex. This means that the distance between the bpy ligands is larger in the cyano complex than in the (CNx) derivative.

Two triplet states of C<sub>2</sub> symmetry (<sup>3</sup>A and <sup>3</sup>B) were found for Ru(bpy)<sub>2</sub>(CN)<sub>2</sub>. Their optimized geometry is almost identical, and the energy difference between them is only 20 cm<sup>-1</sup>. The difference in their electronic structure is that in the <sup>3</sup>A state, the excited electron is on a molecular orbital that is the symmetric, whereas in the <sup>3</sup>B state, it is on an MO, which is the antisymmetric combination of the lowest π\* orbitals of the two bpy ligands. Not surprisingly, the geometries of the two species are very similar. In the equilibrium geometry of the triplet states, the bond lengths are close to those in the singlet state (see Table 1). The length of the Ru–N(6) bond shows only a minor increase, but the Ru–N8 bond, which is cis to CN, becomes longer by 0.015 Å. The C2–Ru–C3 angle in the triplet state is larger, whereas the N6(bpy)–Ru–N7(bpy') angle is much smaller than in the singlet. These differences indicate that the bpy ligands move toward each other due to singlet-to-triplet excitation. This is clearly seen in the decrease in the C(18)–C(19) distance. The investigation of the molecular orbitals and of the Mulliken atomic charges helps us to understand these changes.

**Electronic Structure. Molecular Orbital Analysis.** While keeping in mind that no strict physical content can be assigned to the Kohn–Sham orbitals obtained in DFT calculations, investigation of their energies and character in our system proves to be instructive. The energy level diagram for Ru(bpy)<sub>2</sub>(CN)<sub>2</sub> in vacuum, CCl<sub>4</sub>, and water is shown in Figure 2. The numerical values of the orbital energies can be found in Table 1 of the Supporting Information. In the following, the character of the orbitals will be discussed in terms of the percentage contribution of the basic units (Ru, CN, and bpy) of the complex to each MO, calculated as the sum-of-squares of the MO coefficients of each unit as compared to that of all AOs. The contributions to the most important MOs are shown for Ru(bpy)<sub>2</sub>(CN)<sub>2</sub> in vacuum and in water in Figure 3. The three highest occupied MOs (HOMO to HOMO-2) of the ground state complex in all solvents are assigned as mainly metal-centered d orbitals (contributing around 70%) with small contributions from ligand-centered π orbitals. The HOMO and the two orbitals below it become more dominantly metallic orbitals if the solvent becomes more polar: the contribution from the metal d orbitals increases (from about 66–68% in vacuum to 73–75% in water) at the price of the decrease in the contribution of CN-centered π

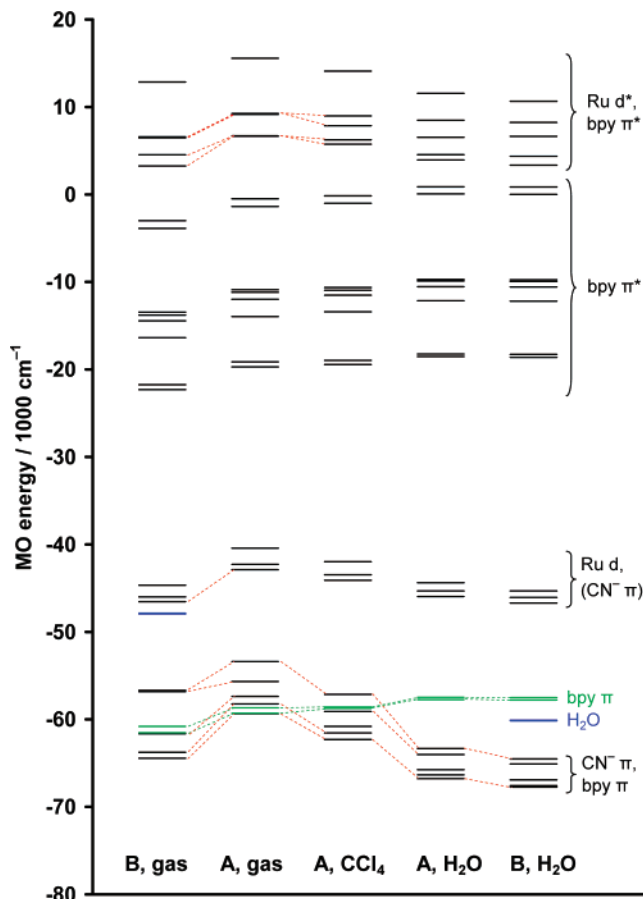


**Figure 2.** MO energy levels and assignments in Ru(bpy)<sub>2</sub>(CN)<sub>2</sub> (A) and in Ru(bpy)<sub>2</sub>(CN)<sub>2</sub>·2H<sub>2</sub>O (B) in vacuum, in a slightly apolar and in a protic polar solvent.

orbitals (from 13–20% to 8–12%, respectively), whereas that from the bpy-centered π orbitals remains constant (at 12–18%). The eight lowest unoccupied MOs (LUMO to LUMO+7) are bpy π\* orbitals. Two high-lying occupied MOs have strong bpy π character (HOMO-7, HOMO-8 in vacuo, shifted to HOMO-3, HOMO-4 in water). The other occupied MOs in the HOMO-4 to HOMO-9 range are mainly CN-ligand-centered π orbitals (with 60–80% contribution to the corresponding MOs) and partly π orbitals centered on the bpy ligands. With the increase in solvent–solute interaction (gas phase < CCl<sub>4</sub> < water), the energies of both the occupied and the unoccupied bpy-centered MOs slightly increase, but the energy difference between them remains essentially unchanged. On the other hand, the energies of the Ru-centered d-type orbitals and the CN-localized MOs decrease with increasing solvent effect. The consequence of the two effects is that the HOMO–LUMO gap increases so that it is larger by 5000 cm<sup>-1</sup> in water than in vacuum. The more contribution from CN orbitals characterizes an MO, the larger the reduction is of the orbital energy in a polar solvent with respect to that in vacuum.

**Charge Distribution.** Figure 4 shows the cumulative Mulliken charges (measured in atomic units; 1 au = 1 electron charge) consisting of the contributions of the atoms of the main units (Ru central atom, CN<sup>-</sup>, and bpy ligands) in the singlet ground state of the Ru(bpy)<sub>2</sub>(CN)<sub>2</sub> complex in gas phase and in 11 different solvents as a function of the solvent's acceptor number (AN).<sup>40</sup> As expected, the solvent influences the charges of the ligands much more than that of the central atom. The charge on the Ru atom is almost the same in all solvents (0.690–0.713) and shows only a small decrease relative to the calculated charge

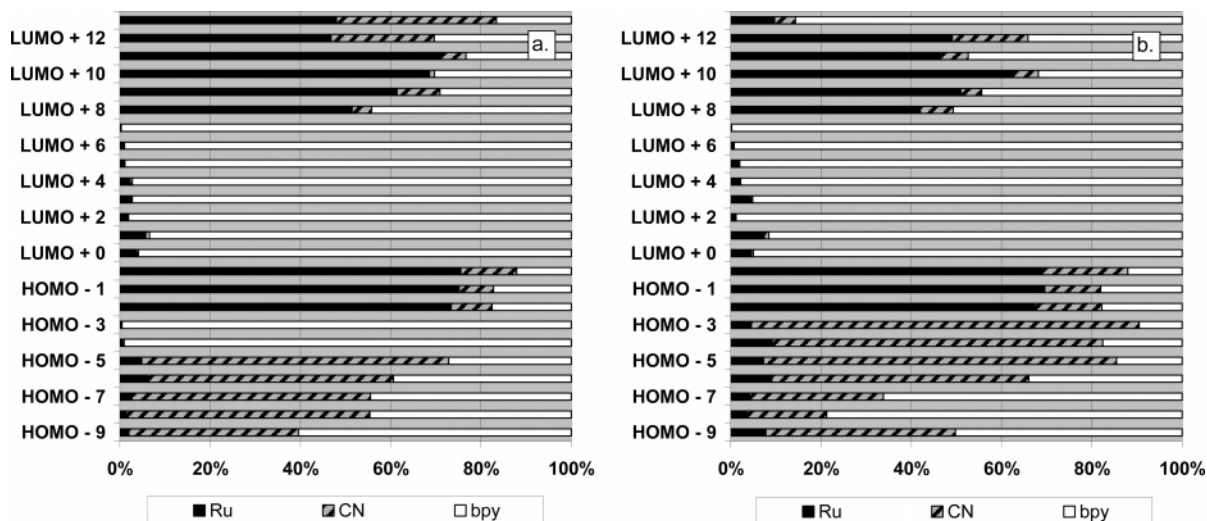


**Figure 3.** The contribution of the atomic orbitals of the Ru, CN, and bpy units to the highest-lying occupied and lowest-lying unoccupied molecular orbitals of  $\text{Ru}(\text{bpy})_2(\text{CN})_2$  in water (a) and in vacuum (b). See text for details of method of calculation.

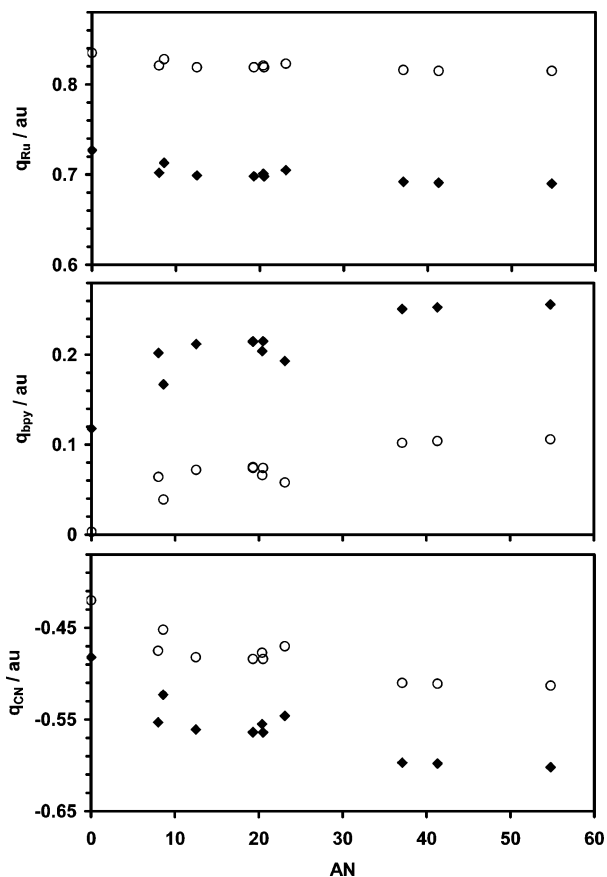


**Figure 4.** Charges (in units of electron charge) on the main units of  $\text{Ru}(\text{bpy})_2(\text{CN})_2$  complex in the singlet ground state (filled symbols) and the triplet ( $^3\text{B}$ ) state (open symbols) in various solvents as a function of the solvent's acceptor number, AN.

in the gas phase (0.727). The positive charge on the bpy ligands and the magnitude of the negative charge on the CN ligands increases with strengthening of the solute–solvent interaction as the polarity of the solvent increases. Using numerical measures of solvent properties, such as the relative permittivity ( $\epsilon$ ) or Gutmann's acceptor number (AN) (used in Figure 4), the correlation is not linear. The largest “charge separation” between the cyano and bpy ligands can be seen in protic solvents ( $\text{H}_2\text{O}$ ,  $\text{MeOH}$ ,  $\text{EtOH}$ ). The increase in the charge separation corresponds to an enhancement of the dipole moment of the

complex, resulting from the polarization induced by the polarizing solvent.

When exciting the singlet ground state of  $\text{Ru}(\text{bpy})_2(\text{CN})_2$  to the lowest-lying triplet state, the charge of the metal center increases by  $\sim 0.12$ , each CN ligand becomes less negative by about 0.08, and the bpy ligand becomes less positive by 0.14 on average (see Figure 4). The dominant consequence of excitation is the charge transfer from the metal center to the bpy ligand. The reduction of the magnitude of the negative charge on CN indicates that excitation induces electron transfer not only in the Ru-to-bpy direction but also from the CN ligand to Ru. Because the bpy ligands have a relatively small positive charge in the ground state, the metal-to-ligand charge transfer (MLCT) excitation reduces their charge close to zero in the triplet. As a consequence, the repulsion between them is reduced with respect to the singlet state, which is reflected in the closer separation between the bpy planes mentioned in the section on molecular geometry.

The change of the charge on the three units of the triplet-state complex due to solvation is similar to that in the singlet state. The charge on the central atom remains essentially the same as in vacuum (the change is  $-0.01$  to  $-0.02$ ) independently of the polarity of the solvent. In the triplet state, similarly to the singlet state, the charge separation between the bpy and CN ligands increases as the solvent becomes more polar (by  $0.07$ – $0.19$ ), but the effect is 30% smaller in the triplet state.

There is a good correlation between the contribution of the CN group to various MOs (Figure 3), the energy of the MO (shown in Figure 2), and charge of the group (as can be seen in Figure 4). Namely, with the increase in the solute–solvent interaction, the energies of the CN-centered orbitals decrease significantly, and the charge on the CN groups increases. At the same time, the CN  $\pi$  contribution to the top three occupied, predominantly Ru d-type MOs decreases, yielding a less expressed reduction of MO energies than that of “pure” CN orbitals and a minimal change of the charge of the unit on which the orbitals are localized, Ru. Similarly, the mixing of CN orbitals to MOs that are predominantly bpy  $\pi$  orbitals decreases with the solvent effect. In this case, however, the energy of the MO increases as the solute–solvent interaction increases, and the number of electrons assigned by Mulliken population analysis to the orbital decreases, being one of the reasons why the charge of the bpy units becomes more positive. The solvent-induced polarization of the molecule is the common reason for

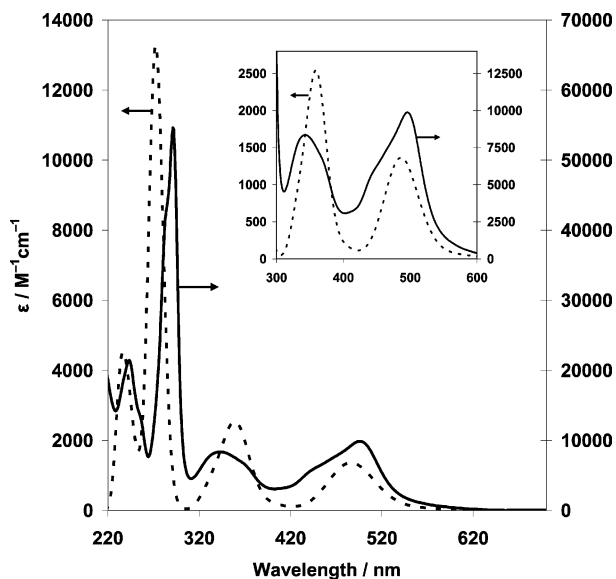


**Figure 5.** The simulated (dashed line) and measured (solid line) absorption spectra of Ru(bpy)<sub>2</sub>(CN)<sub>2</sub> in acetonitrile (line width,  $\sigma = 1000 \text{ cm}^{-1}$ ).

the shift of the orbital energies and the change of the charges on each unit, culminating in the change of the dipole moment.

**Electronic Absorption by the Singlet Ground-State Complex.** The actual differences of the excited energy levels and that of the ground state, as predicted by TD-DFT, are not identical to the differences in the energies of orbitals involved in various orbital-to-orbital transitions. The reason is partly that the transitions corresponding to excitation from one electronic level to another are composed of several orbital-to-orbital excitations, often with commensurable weight, and partly the fact that the molecule's energy is not the sum of the energies of the occupied orbitals. Yet, from the changes of MO energies, one can expect that the increase in the HOMO–LUMO gap and in neighboring orbital pairs induces a blue shift of the lowest energy band of the absorption spectrum with the increase in solvent polarity. The energies and oscillator strengths have been calculated for the 40 lowest-energy transitions of Ru(bpy)<sub>2</sub>(CN)<sub>2</sub> in the gas phase and in 11 solvents. From these data, the absorption spectra were simulated by the procedure described in the computational section. A sample spectrum is shown in Figure 5, and the location of the maxima of the simulated spectra are listed in Table 3. The spectra are characterized by generally three bands, which is in good agreement with the experiment. All bands whose maxima correspond to energies smaller than  $33\,000 \text{ cm}^{-1}$  are composed of contributions from transitions from the three highest occupied MOs, which are predominantly of Ru d character, to one or more of the lowest six unoccupied MOs that are bpy  $\pi^*$  orbitals. There are two bands in almost all spectra in this range, indicating that the two longest-wavelength bands correspond to MLCT. The maximum of the MLCT<sub>1</sub> band is shifted from 563 nm in vacuum to 460 nm in water, whereas that of the MLCT<sub>2</sub> band is moved from 391 to 343 nm, respectively. The MLCT<sub>2</sub> band often overlaps with the next lowest-energy band, the location of whose maximum (273 nm) slightly depends on the solvent. This third band corresponds to bpy  $\pi \rightarrow$  bpy  $\pi^*$  (LL) transitions. The calculated spectra agree well with the experiment. Not only the location of the maxima but also the shape of the bands is reproduced. The largest difference between the experimental and theoretical data is found in the molar absorption coefficients, the calculated results being a factor of 5 larger.

**TABLE 2: Location of the Measured and Calculated Maxima of MLCT Absorption Bands of the Ru(bpy)<sub>2</sub>(CN)<sub>2</sub> Complex**

solvent	AN	$F(\epsilon, n)$	$\lambda_{\text{Ab1}}$ nm <sup>a</sup>	$l_{\text{Ab2}}$ nm <sup>a</sup>	$\lambda_{\text{Ab1m}}$ nm <sup>a</sup>	$\lambda_{\text{Ab2m}}$ nm <sup>a,b</sup>
water	54.8	0.3199	460	343	431	
methanol	41.3	0.3083	462	344	459 <sup>b</sup>	321
ethanol	37.1	0.2887	464	346	469 <sup>b</sup>	328
chloroform	23.1	0.1509	501	367	498	342
nitromethane	20.5	0.2918	486	359	492 <sup>b</sup>	
CH <sub>2</sub> Cl <sub>2</sub>	20.4	0.2172	493	362	501	344
acetonitrile	19.3	0.3050	486	359	494	343
DMSO	19.3	0.2632	486	359	502 <sup>b</sup>	347
acetone	12.5	0.2842	488	360	511 <sup>b</sup>	349
CCl <sub>4</sub>	8.6	0.0101	522	376		
THF	8	0.2093	495	364	528 <sup>b</sup>	358
gas phase			563	391		

<sup>a</sup>  $\lambda_{\text{Ab1}}$  and  $\lambda_{\text{Ab2}}$  are the calculated, the  $\lambda_{\text{Ab1m}}$  and  $\lambda_{\text{Ab2m}}$  correspond to the measured MLCT<sub>1</sub> and MLCT<sub>2</sub> absorption band maxima. <sup>b</sup> From ref 9.

To quantify the correlation between the location of spectral maxima and solvent properties, we tested two commonly used indexes characterizing various solvents. One of these is the solvent dielectric parameter ( $F$ ), which represents the dielectric polarity of the solvent around the polar solute.<sup>41,42</sup> The other is Guttmann's acceptor number (AN),<sup>40</sup> which measures the electron acceptor character of the solvent.  $F$  is a function of the relative permittivity ( $\epsilon$ ) and the refraction index ( $n$ ) of the solvent:

$$F = \frac{\epsilon - 1}{2\epsilon + 1} - \frac{n^2}{2n^2 + 1}$$

One can expect the location of spectral maxima calculated with the CPCM method, which characterizes the polarity of the solvent by these same parameters, to show good correlation with the  $F$  parameter. The actual correlation, shown in Figure 6a proved to be acceptable for aprotic solvents for both MLCT bands but is poor for protic solvents. The measured band maxima, however, correlate poorly with  $F$ . On the other hand, the correlation of the location of the experimental band maxima with the acceptor number (see Figure 6b) is exceptionally good ( $R^2 = 0.98$ ), and that of the calculated data is also better with the AN than with the  $F$  parameter. The slopes of the lines fitted to the experimental and theoretical data are different. The same observation was made by Stoyanov et al.<sup>23</sup> in their studies of the spectral characteristics of Ru(bpy)<sub>2</sub>(CNPhMe<sub>2</sub>)<sub>2</sub>. The experimental slope is larger than the theoretical: the calculated band maxima as compared to the experiments are at energies about  $2000 \text{ cm}^{-1}$  lower in high-AN solvents and about  $1500 \text{ cm}^{-1}$  higher in less polar solvents. The correlation between the calculated and experimental band maxima is quite good, close to linear.

Because the solvent induces a shift of charge in the complex, one expects a correlation between the charges of the units of the complex and the location of the spectral maxima. For the calculated spectra, the correlation of the charge difference between the Ru atom and bpy ligands and the location of the band maxima is excellent ( $R^2 > 0.99$ ), so strong that it can be used for prediction. The correlation of the measured band maxima with the charge, however, is not as good. One can interpret the strong correlation between the calculated charge difference and band maximum as the consequence of the correlation of the charges of the units and the MO energies, as mentioned earlier.

**TABLE 3: The Location of the MLCT Band Maxima and the Charge of the Main Units of Coordinated  $\text{Ru}(\text{bpy})_2(\text{CN})_2$  (A) Complexes, A  $\times$  S**

complex	medium	MLCT <sub>1</sub> , nm	MLCT <sub>2</sub> , nm	charge of Ru	charge of CN <sup>a</sup>	charge of bpy <sup>b</sup>	charge of S
Measured							
A	water	431	(sh)				
A	1 M H <sub>2</sub> SO <sub>4</sub>	410					
A	MeCN	494	343				
Calculated ( $\sigma = 1000 \text{ cm}^{-1}$ )							
A	gas phase	563	391	0.727	-0.482	0.118	
A $\times$ 2H <sub>2</sub> O	gas phase	529	378	0.711	-0.443	0.165	-0.077
A $\times$ H <sub>3</sub> O <sup>+</sup>	gas phase	460	344	0.705	-0.448	0.292	0.552
A $\times$ H <sup>+</sup>	gas phase	443	330	0.707	-0.375	0.273	
A $\times$ 2H <sub>3</sub> O <sup>+</sup>	gas phase	368		0.701	-0.433	0.329	0.381
A $\times$ 2H <sup>+</sup>	gas phase	331		0.710	-0.299	0.315	
A $\times$ 2MeCN	gas phase	539	385	0.719	-0.339	0.415	0.574
A	water	460	343	0.690	-0.249	0.488	0.406
A $\times$ 2H <sub>2</sub> O	water	447	335	0.683	-0.472	0.151	-0.038
A $\times$ H <sub>3</sub> O <sup>+</sup>	water	409		0.694	-0.602	0.256	
A $\times$ H <sup>+</sup>	water	391		0.696	-0.534	0.279	-0.086
A $\times$ 2H <sub>3</sub> O <sup>+</sup>	water	359		0.684	-0.398	0.355	
A $\times$ 2H <sup>+</sup>	water	341		0.714	-0.554	0.374	0.450
A	MeCN	486	359	0.698	-0.353	0.387	
A $\times$ 2MeCN	MeCN	476	351	0.690	-0.373	0.450	0.582
					-0.300	0.465	0.467
					-0.564	0.214	
					-0.553	0.247	-0.039

<sup>a</sup> For nonsymmetric complexes, the upper and lower charge values correspond to the noncoordinated and the coordinated CN ligand, respectively.

<sup>b</sup> For nonsymmetric complexes, the upper and lower charge values correspond to the bpy ligand trans to the coordinated and to the noncoordinated CN ligand, respectively.

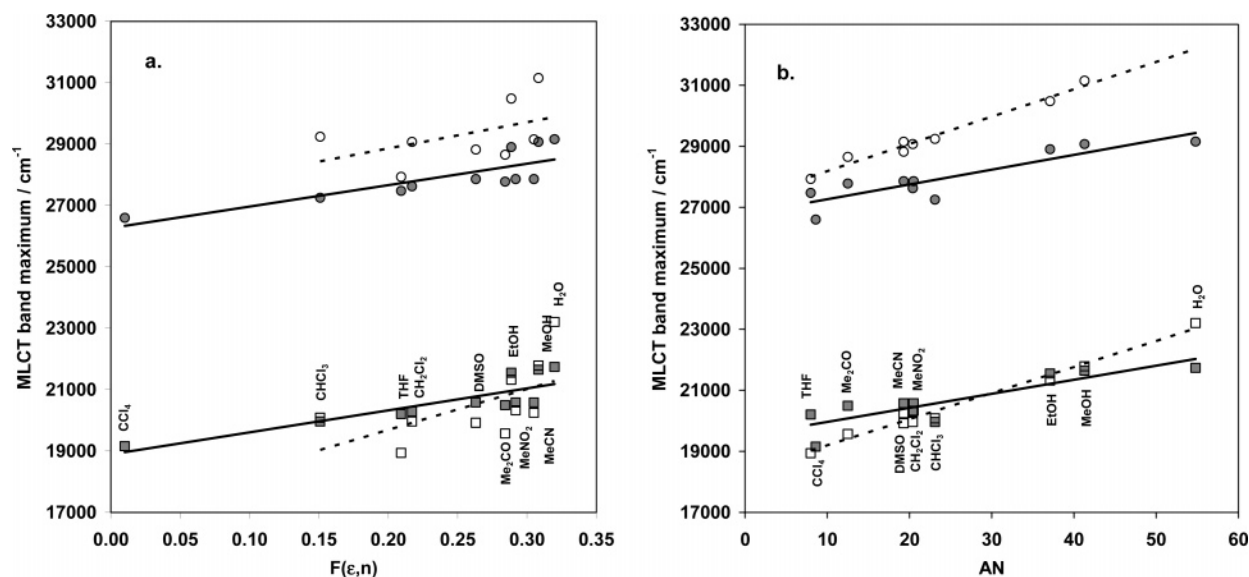


**Figure 6.** The solvent dependence of the location of the maxima of the MLCT<sub>1</sub> (circles) and the MLCT<sub>2</sub> (squares) bands of  $\text{Ru}(\text{bpy})_2(\text{CN})_2$ . Plotted is the measured (open symbols, dashed lines) and calculated (filled symbols, continuous lines) location of band maximum as a function of (a) parameter  $F$  and (b) the acceptor number of the solvent. The lines are fitted by linear regression.

In more polar solvents—in particular, in protic solvents—the molecules of the solvent as individual particles may interact with various sites of the complex, inducing changes in the electronic structure of the ligands. This effect goes beyond those that can be caused by a simple dielectric solvent as a polarizable continuum, and one can expect that the CPCM model will not describe this specific solute–solvent interaction. The analysis of group charges in  $\text{Ru}(\text{bpy})_2(\text{CN})_2$  support the expectation that the largest negative charge is localized on the cyano ligands. This charge is large and makes the CN ligands strong Lewis base centers of the molecule. Molecules of protic solvents are expected to form a hydrogen bond with such centers, or if the acidity of the solvent is large enough, even complete protonation of the nitrogen site of ligands can take place. Our measurements

show that the spectrum *does* change due to protonation: if the neutral aqueous solution of  $\text{Ru}(\text{bpy})_2(\text{CN})_2$  is made acidic (1 M H<sub>2</sub>SO<sub>4</sub>), the MLCT band is shifted to higher transition energies (see Figure 7). To understand the role of such interactions we calculated the structure and spectra of complexes in which solvent particles “coordinate” one or both cyano groups:  $\text{Ru}(\text{bpy})_2(\text{CN})_2 \times \text{H}^+$  and  $\text{Ru}(\text{bpy})_2(\text{CN})_2 \times \text{H}_3\text{O}^+$  in the former and  $\text{Ru}(\text{bpy})_2(\text{CN})_2 \times 2\text{H}_2\text{O}$ ,  $\text{Ru}(\text{bpy})_2(\text{CN})_2 \times 2\text{MeCN}$ ,  $\text{Ru}(\text{bpy})_2(\text{CN})_2 \times 2\text{H}_3\text{O}^+$ , and  $\text{Ru}(\text{bpy})_2(\text{CN})_2 \times 2\text{H}^+$  in the second group (see Figures 7 and 8). The spectra were evaluated both in vacuum and in water (or in acetonitrile if the coordinated molecule is CH<sub>3</sub>CN) as solvent. In principle, by comparing the spectra of the bare complex and  $\text{Ru}(\text{bpy})_2(\text{CN})_2 \times 2\text{H}_2\text{O}$  in vacuum and in water solvent, one could determine whether water

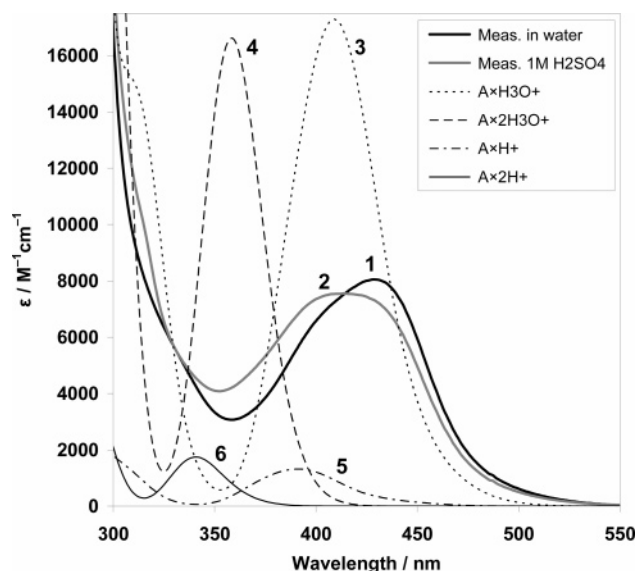


**Figure 7.** The measured absorption spectrum of Ru(bpy)<sub>2</sub>(CN)<sub>2</sub> (A) in neutral water (1) and in 1 M H<sub>2</sub>SO<sub>4</sub> (2), as well as the simulated spectra of A×H<sub>3</sub>O<sup>+</sup> (3), A×2H<sub>3</sub>O<sup>+</sup> (4), A×H<sup>+</sup> (5), and A×2H<sup>+</sup> (6) from the TD-DFT transition energies calculated in water continuum solvent.

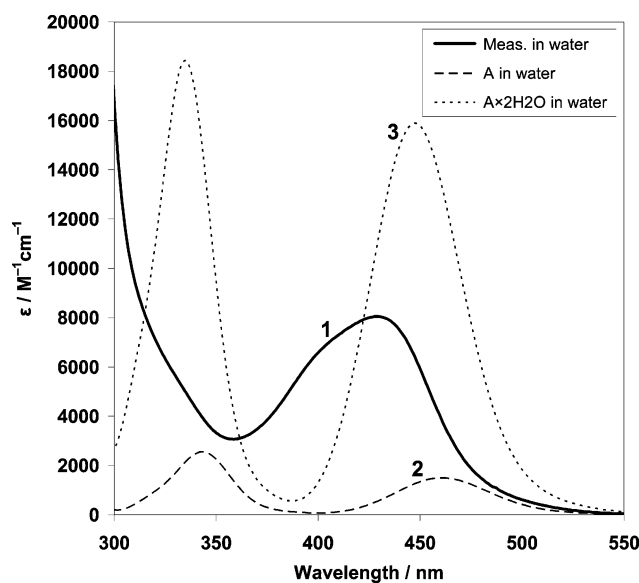


**Figure 8.** The measured absorption spectrum of Ru(bpy)<sub>2</sub>(CN)<sub>2</sub> (A) in water (1) and the simulated spectra of A (2) and A×2H<sub>2</sub>O (3) from the TD-DFT transition energies calculated in water continuum solvent.

as a dielectric continuum or H<sub>2</sub>O as a coordinating molecule is more important in the spectral change.

In the Ru(bpy)<sub>2</sub>(CN)<sub>2</sub>×2H<sub>2</sub>O complex, the H atom forming the hydrogen bond is closer to the O atom than to the N of CN. If the “solvent” carries an extra proton (H<sub>3</sub>O<sup>+</sup>), the bridging H atom is highly charged and is essentially transferred from the O atom to N ( $r(\text{N}-\text{H}^+) = 1.071 \text{ \AA}$ ,  $r(\text{H}^+-\text{O}) = 1.495 \text{ \AA}$ ). This N–H<sup>+</sup> distance is essentially the same as when a bare proton is connected to the CN group ( $r(\text{N}-\text{H}^+) = 1.001 \text{ \AA}$ ). If CH<sub>3</sub>-CN is coordinated to the CN group, the H atom remains far from the N atom, just as if the solvent molecule is water (where  $r(\text{N}-\text{H}) = 2.168 \text{ \AA}$ ). The H<sub>2</sub>O molecules in Ru(bpy)<sub>2</sub>(CN)<sub>2</sub>×2H<sub>2</sub>O and in water solvent abstract about 0.08 electron charge from the complex. This electron withdrawal not only reduces the negative charge of the CN ligands but also extends as far as the bpy ligands, which become more positive. At the same time, the energies of the top three occupied MOs decrease,

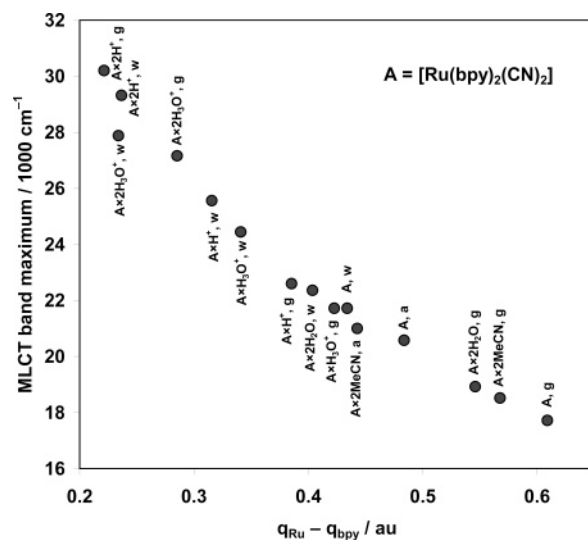


**Figure 9.** The correlation between the location of the MLCT<sub>1</sub> absorption maximum of Ru(bpy)<sub>2</sub>(CN)<sub>2</sub>×S (S: 2H<sub>2</sub>O, H<sub>3</sub>O<sup>+</sup>, 2H<sub>3</sub>O<sup>+</sup>, H<sup>+</sup>, 2H<sup>+</sup>, and 2MeCN) complex in water (w) and acetonitrile (a) as well as in the gas phase (g) and the difference between the charge of Ru atom and the average of charges of bpy ligands of the ground state complex.

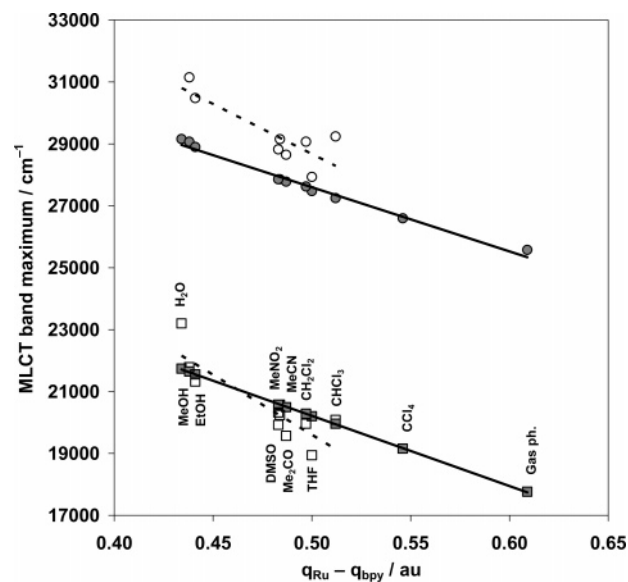


**Figure 10.** The correlation between the location of the MLCT<sub>1</sub> (squares) and the MLCT<sub>2</sub> (circles) absorption maxima and the difference between the charge of Ru atom and the average of charges of bpy ligands of the ground state complex in different solvents. The open symbols and dashed lines represent the measured; the filled symbols and continuous lines, the calculated data. The lines are fitted by linear regression.

resulting in the increase in the energy of the MLCT electronic transition. Figure 8 shows that the molecular interaction of the complex and H<sub>2</sub>O, similar to the continuum solvent, shifts the absorption bands. Table 3 shows the location of the simulated MLCT<sub>1</sub> band maximum in the coordinated complexes studied. The maximum is shifted by ~1140 cm<sup>-1</sup> due to coordination of a H<sub>2</sub>O molecule to both cyano groups in vacuum. If the complex is put into water, the shift is almost 4000 cm<sup>-1</sup>. The coordination of two H<sub>2</sub>O molecules in addition to the continuum solvent shifts the band maximum by an additional 630 cm<sup>-1</sup>, as compared to the non-coordinating solvent itself. The effect due to the continuum solvent is larger than that due to coordination by neutral solvent molecules. The influence of molecular and continuum acetonitrile on the spectral shift is

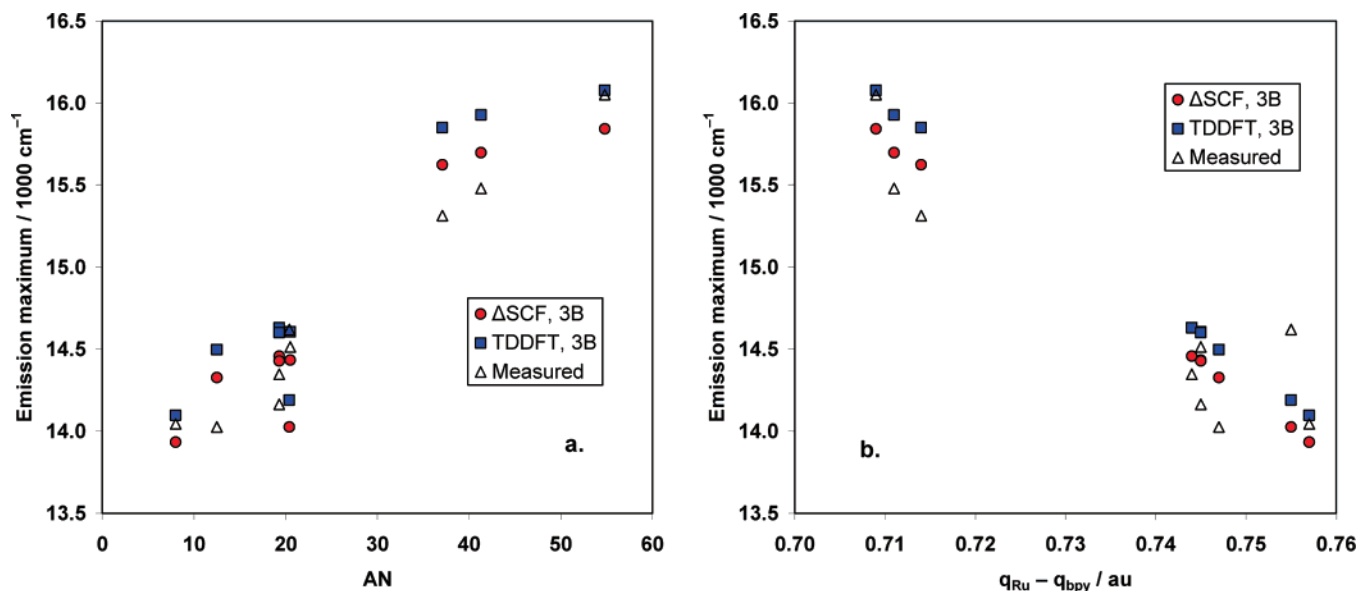


**Figure 11.** The change of the location of the emission maximum of  $\text{Ru}(\text{bpy})_2(\text{CN})_2$  with the AN (a) as well as its correlation with the calculated charge difference between the Ru atom and the bpy ligand in the triplet ( $^3\text{B}$ ) state (b).

smaller than that of water: the analogous numbers are 790, 2810, and  $432\text{ cm}^{-1}$ , respectively. The spectral shift and the charge distribution of the complex are in a close correlation, despite the complex interplay between the charge shift induced by the solvent and the coordinating  $\text{H}_2\text{O}$  molecule. As Table 3 shows, the continuum solvent itself enhances the charges of the CN and bpy units, moving the charges in the opposite direction. The coordinating  $\text{H}_2\text{O}$  molecule, instead, shifts both charges in the same direction as it removes some charge from whole complex. Both interactions induce a very small decrease in the positive charge on the central atom. At the same time, both the induced dipole enhancement and the charge removal result in a spectral blue shift. This is not surprising because the charge on the bpy units increases due to both effects. As a consequence, the charge difference between Ru and bpy, which one expects to be closely related to the energy of the MLCT transitions, is reduced. Plotted in Figures 9 and 10 are the correlation between the energy corresponding to the MLCT<sub>1</sub> maximum and the Ru–bpy charge difference. The larger the difference, the smaller the energy of the transition, in agreement with the expectation and the picture seen in connection with the polarization effect of various solvents. The charge and spectral shift caused by the coordinating  $\text{H}_2\text{O}$  fits well the tendency seen in the case of the solvent series. On the other hand, if one or both CN group is coordinated by a proton or hydroxonium, the slope of the correlation is steeper, indicating that the additional charge introduces more profound changes in the electronic structure of the complex.

The importance of the additional effect of protic solvents on the complex, namely, partial or full protonation of the Lewis base center of the complex, is indicated by the change of the experimental spectrum that is observed when the pH of the water solvent is reduced (see Figure 7). To analyze the effect of partial and full protonation, TD-DFT calculations were performed on  $\text{Ru}(\text{bpy})_2(\text{CN})_2$  coordinated by (a) hydroxonium ions at one or both cyano groups and (b) protonated at one or both cyanide ligands. The first hydrogen-bonded hydroxonium ion induces a significant spectral blue shift with respect to the bare complex in vacuum,  $4000\text{ cm}^{-1}$  in vacuum and  $6690\text{ cm}^{-1}$  in water. If, in addition, the other CN group is also coordinated by a hydrogen-bonded hydroxonium ion, the shift is enhanced to  $9410\text{ cm}^{-1}$  in vacuum and  $10\,093\text{ cm}^{-1}$  in water. The negative

**TABLE 4: Measured Maxima of Emission Spectra and Calculated Energy Difference of Triplet ( $^3\text{A}$  and  $^3\text{B}$ ) and Singlet State of  $\text{Ru}(\text{bpy})_2(\text{CN})_2$  Complex<sup>a</sup>**

solvent	AN	$\nu_{3\text{B},\text{SCF}}^*$ <sup>b</sup>	$\nu_{3\text{A},\text{SCF}}^*$ <sup>b</sup>	$\nu_{3\text{B},\text{TD}}^*$ <sup>c</sup>	$\nu_{3\text{A},\text{TD}}^*$ <sup>c</sup>	$\nu_{\text{meas}}^*$ <sup>d</sup>
water	54.8	15.84	15.66	16.08	15.78	16.05
methanol	41.3	15.70	15.52	15.93	15.63	15.48
ethanol	37.1	15.62	15.45	15.85	15.55	15.31
chloroform	23.1	13.61	13.46	13.77	13.36	
nitromethane	20.5	14.43	14.26	14.61	14.25	14.51
$\text{CH}_2\text{Cl}_2$	20.4	14.03	13.86	14.19	13.81	14.62
acetonitrile	19.3	14.43	14.26	14.60	14.24	14.16
DMSO	19.3	14.46	14.29	14.63	14.27	14.35
acetone	12.5	14.33	14.16	14.50	14.13	14.03
$\text{CCl}_4$	8.6	12.62	12.49	12.74	12.28	
THF	8	13.93	13.77	14.10	13.71	14.04
gas phase		10.83	10.74	10.78	10.31	

<sup>a</sup> All energy value are given in  $1000\text{ cm}^{-1}$ . <sup>b</sup>  $\nu_{3\text{A},\text{SCF}}^*$  and  $\nu_{3\text{B},\text{SCF}}^*$  are energy differences calculated using the  $\Delta\text{SCF}$  method for the  $^3\text{A}$  and  $^3\text{B}$  states, respectively. <sup>c</sup>  $\nu_{3\text{A},\text{TD}}^*$  and  $\nu_{3\text{B},\text{TD}}^*$  are calculated energy differences with TDDFT for  $^3\text{A}$  and  $^3\text{B}$  states respectively. <sup>d</sup> From ref 9.

charge on the cyanide group involved in this interaction is reduced by 0.12 or 0.14 in vacuum and 0.09 and 0.11 in water, respectively, when one or two hydroxonium ions are considered. This shift is transmitted to the bpy group, where the effect is accentuated: the positive charge on bpy increases more than on CN. Protonation of the complex draws even more electron density from the CN group, by as much as 0.18 in water solvent as compared to the bare complex in vacuum, and 0.35 additional positive charge appears on the bpy units. The consequence is a very large blue shift:  $11\,560\text{ cm}^{-1}$ . The magnitude of this shift is much larger than what is experimentally observed, which suggests that this model overemphasizes the protonation effect. As expected, the sharing of the proton between the complex and a solvent molecule, modeled by coordination of  $\text{H}_3\text{O}^+$ , yields a more realistic spectral shift. The simulated spectrum of the singly and the doubly hydroxonium coordinated complex calculated in water solvent, as well as the measured spectra in neutral aqueous solution and in 1 M  $\text{H}_2\text{SO}_4$ , are also shown in Figure 7. The comparison shows that the complex exists mostly in partially protonated form in acidic solutions.

**Emission Spectra from the Triplet Excited States.** The solvent effect on the energy difference between the triplet and

singlet state at the triplet equilibrium geometry significantly influences the location of the maximum on the phosphorescence spectrum. These energy differences in various solvents calculated by the TD-DFT and  $\Delta$ SCF methods, together with the energies corresponding to the measured emission maxima, are shown in Figure 11 as a function of the solvent acceptor number as well as of the Ru–bpy charge difference calculated for the triplet molecule in each solvent. Both the theoretical and the experimental emission energies are in good correlation with the acceptor number of the solvent. The energies calculated by  $\Delta$ SCF agree with the experiment within 100–300 cm<sup>-1</sup>, that is, within experimental accuracy. Those obtained by TD-DFT are  $\sim$ 2000 cm<sup>-1</sup> higher than the measured data. There is no sound theoretical basis to decide which calculation is more reliable. TD-DFT uses perturbation theory to take into account the distortion of the electronic structure due to the electromagnetic field and often provides very good estimates.  $\Delta$ SCF, on the other hand, is based on the fact that the Hohenberg–Kohn theorem is valid for each spin multiplet state separately. Because both methods are approximate, we think that it is reasonable to make a comparison with experiment for a given, relatively narrow class of compounds and, on the basis of that, use the method that proves to provide better agreement with the experiment. In the present case,  $\Delta$ SCF fulfils this role.

It is remarkable that the solvent dependence of the emission energies is much better described by the CPCM method than that of the absorption energies of the ground singlet state of the complex. In particular, the T  $\rightarrow$  S energy differences are just as well described in protic solvents as in aprotic ones. This can be understood by noting that the electron density on the CN ligand is smaller in the triplet than in the singlet state. As a result, the direct donor–acceptor interaction (or partial or total protonation at the cyano ligand) is weak in the triplet state. The reason why the CPCM results agree better with the experiment for triplet emission than for singlet absorption is that the direct “chemical” interaction, which is not directly taken into account by CPCM, is smaller in the emitting triplet state than in the absorbing singlet. Just like the absorption energies, the location of the calculated (and less strongly, the measured) emission maxima is very well correlated with the difference of the charges on Ru and bpy in the triplet state (Figure 11b). However, because this difference changes more slowly with the increase in solvent polarity than that in the singlet state, the location of the maximum of the emission spectrum is shifted more slowly as a function of the polarity of the solvent than that of the singlet–singlet absorption, explaining the experimental observation.

## Conclusions

Our TD-DFT calculations for a prototype ruthenium-bis-(diimine) complex, performed for solvents of various polarity as described by the CPCM model, yielded good agreement with the experiment for the location of the maxima of the MLCT absorption and emission bands. On the basis of the electronic structure calculations, the solvent shift is shown to be strongly correlated to the charge difference between the Ru central atom and the bpy ligands. The MLCT excitation transfers an electron from a predominantly metal d orbital to a bpy  $\pi^*$  orbital. The energy of the occupied orbital is closely related to the Ru–bpy charge difference: the more charge is located on an MO, the lower the MO energy is. Although the energy of absorption is not identical to the difference in the donor and acceptor MO energies, the dominant factor is this energy difference. As the increasing solute–solvent interaction induces larger and larger

Ru–bpy charge difference, the HOMO–LUMO gap increases, the absorption—and to a smaller extent, the triplet emission—maximum is shifted to higher energies. The location of the maxima is in very good linear correlation with the solvent’s acceptor number, indicating that this index measures well the various factors influencing the “polarity” of the solvent.

We also studied the relative importance of specific solute–solvent interaction, that is, coordination of solvent molecules to the Lewis basic center of the complex, and the effect of the polarizable continuum solvent. The solvent shift induced by the coordination of one or two molecules of a polar solvent (H<sub>2</sub>O or CH<sub>3</sub>CN) to the cyano groups is smaller than the effect caused by the charge separation induced by the continuum polar solvent. On the other hand, by comparing our measured absorption spectra in aqueous solution at low pH with calculated spectra for the bare Ru(bpy)<sub>2</sub>(CN)<sub>2</sub> complex in vacuum, in water solvent as well as the complex coordinated by solvent H<sub>2</sub>O, H<sup>+</sup>, H<sub>3</sub>O<sup>+</sup> at one or both cyano ligands, we found that protonation of the complex (coordination of a proton or H<sub>3</sub>O<sup>+</sup>) exerts so large an influence on the charge distribution of the complex that the spectral blue shift becomes much larger than the effect caused by a continuum solvent.

We found that the applied theoretical approach, TD-DFT with the B3LYP combination of functionals and the LANL2DZ basis set, provides good agreement between experiment and theory so that it can be considered a reasonable basis for understanding the electronic structure background of the specific solute–solvent interaction and, hence, offers a reasonable tool for designing sensitizers.

**Acknowledgment.** Financial support by the Hungarian National Scientific Research Fund (Grant No. K63494) is gratefully acknowledged.

**Supporting Information Available:** Additional information as noted in text. This material is available free of charge via the Internet at <http://pubs.acs.org>.

## References and Notes

- (1) Nazeeruddin, M. K.; Kay, A.; Rodocio, I.; Humphry-Baker, R.; Müller, E.; Liska, P.; Vlachopoulos, N.; Grätzel, M. *J. Am. Chem. Soc.* **1993**, *115*, 6382–6390.
- (2) Hou, Y.; Xie, P.; Wu, K.; Wang, J.; Zhang, B.; Cao, Y. *Sol. Energy Mater. Sol. Cells* **2001**, *70*, 131–139.
- (3) Kalyanasundaram, K.; Grätzel, M. *Coord. Chem. Rev.* **1998**, *77*, 347–414.
- (4) Zakeeruddin, S. M.; Nazeeruddin, M. K.; Pechy, P.; Rotzinger, F. P.; Humphry-Baker, R.; Kalyanasundaram, K.; Grätzel, M. *Inorg. Chem.* **1997**, *36*, 5937–5946.
- (5) DeCola, L.; Balzani, V.; Barigelletti, F.; Flamigni, L.; Belsler, P.; von Zelewsky, A.; Frank, M.; Vögtle, F. *Inorg. Chem.* **1993**, *32*, 5228–5238.
- (6) Balzani, V.; Juris, A.; Venturi, M.; Campagna S.; Serroni, S. *Chem. Rev.* **1996**, *96*, 759–833.
- (7) Denti, G.; Campagna, S.; Serroni, S.; Ciano, M.; Balzani, V. *J. Am. Chem. Soc.* **1992**, *114*, 2944–2950.
- (8) Rampi, M. A.; Indelli, M. T.; Scandola, F.; Pina, F.; Parola, A. J. *Inorg. Chem.* **1996**, *35*, 3355.
- (9) Timpson, C. J.; Bignozzi, C. A.; Sullivan, B. P.; Kober, E. M.; Meyer, T. J. *J. Phys. Chem.* **1996**, *100*, 2915–2925.
- (10) (a) Indelli, M. T.; Ghirelli, M.; Prodi, A.; Chiorboli, C.; Scandola, F.; McClenaghan, N. D.; Puntoriero, F.; Campagna, S. *Inorg. Chem.* **2003**, *42*, 5489–5497. (b) Simpson, N. R. M.; Ward, M. D.; Morales, A. F.; Barigelletti, F. *J. Chem. Soc. Dalton Trans.* **2002**, 2449–2454.
- (11) Amadelli, R.; Argazzi, R.; Bignozzi, C. A.; Scandola, F. *J. Am. Chem. Soc.* **1990**, *112*, 7099–7103.
- (12) Casida, M. E. In *Recent Advances in Density Functional Methods, Part I*; Chong, D. P., Ed.; World Scientific: Singapore, 1995; p 155.
- (13) Bauernschmitt, R.; Ahlrichs, R. *Chem. Phys. Lett.* **1997**, *264*, 573.
- (14) Stratmann, R. E.; Scuseria, G. E. *J. Chem. Phys.* **1998**, *109*, 8218.
- (15) Dreuw, A.; Head-Gordon, M. *Chem. Rev.* **2005**, *105*, 4009–4037.

- (16) Fodor-Kardos, A.; Horváth, A. *Photochem. Photobiol. Sci.* **2005**, *4*, 167–174.
- (17) Guillemoles, J. F.; Barone, V.; Joubert, L.; Adamo, C. *J. Phys. Chem.* **2002**, *106*, 11354–11360.
- (18) Adamo, C.; Barone, V. *J. Chem. Phys.* **1999**, *110*, 6158.
- (19) Klamt, A.; Schüürmann, G. *J. Chem. Soc. Perkins Trans. 2* **1993**, 799.
- (20) Andzelm, J.; Kölmel, C.; Klamt, A. *J. Chem. Phys.* **1995**, *103*, 9312.
- (21) Cossi, M.; Rega, N.; Scalmani, G.; Barone, V. *J. Comput. Chem.* **2003**, *24*, 669.
- (22) Villegas, J. M.; Stoyanov, S. R.; Huang, W.; Lockyear, L. L.; Reibenspies, J. H.; Rillema, D. P. *Inorg. Chem.* **2004**, *43*, 6383–6396.
- (23) Stoyanov, S. R.; Villegas, J. M.; Rillema, D. P. *Inorg. Chem. Commun.* **2004**, *7*, 838–841.
- (24) De Angelis, F.; Fantacci, S.; Selloni, A. *Chem. Phys. Lett.* **2004**, *389*, 204–208.
- (25) Fantacci, S.; De Angelis, F.; Sgamellotti, A.; Re, N. *Chem. Phys. Lett.* **2004**, *396*, 43–48.
- (26) De Angelis, F.; Fantacci, S.; Selloni, A.; Nazeeruddin, M. K. *Chem. Phys. Lett.* **2005**, *415*, 115–120.
- (27) Joubert, L.; Guillemoles, J. F.; Adamo, C. *Chem. Phys. Lett.* **2003**, *371*, 378–385.
- (28) Ciofini, I.; Daul, C. A.; Adamo, C. *J. Phys. Chem.* **2003**, *107*, 11182–11190.
- (29) Demas, J. N.; Turner, T. F.; Crosby, G. A. *Inorg. Chem.* **1969**, *8*, 674–675.
- (30) Becke, A. D. *J. Chem. Phys.* **1993**, *98*, 5648.
- (31) Lee, C.; Yang, W.; Parr, R. G. *Phys. Rev. B: Condens. Matter Mater. Phys.* **1988**, *37*, 785.
- (32) Hay, P. J.; Wadt, W. R. *J. Chem. Phys.* **1985**, *82*, 270.
- (33) Wadt, W. R.; Hay, P. J. *J. Chem. Phys.* **1985**, *82*, 284.
- (34) Hay, P. J.; Wadt, W. R. *J. Chem. Phys.* **1985**, *82*, 299.
- (35) Frisch, M. J.; Trucks, G. W.; Schlegel, H. B.; Scuseria, G. E.; Robb, M. A.; Cheeseman, J. R.; Montgomery, J. A., Jr.; Vreven, T.; Kudin, K. N.; Burant, J. C.; Millam, J. M.; Iyengar, S. S.; Tomasi, J.; Barone, V.; Mennucci, B.; Cossi, M.; Scalmani, G.; Rega, N.; Petersson, G. A.; Nakatsuji, H.; Hada, M.; Ehara, M.; Toyota, K.; Fukuda, R.; Hasegawa, J.; Ishida, M.; Nakajima, T.; Honda, Y.; Kitao, O.; Nakai, H.; Klene, M.; Li, X.; Knox, J. E.; Hratchian, H. P.; Cross, J. B.; Bakken, V.; Adamo, C.; Jaramillo, J.; Gomperts, R.; Stratmann, R. E.; Yazyev, O.; Austin, A. J.; Cammi, R.; Pomelli, C.; Ochterski, J. W.; Ayala, P. Y.; Morokuma, K.; Voth, G. A.; Salvador, P.; Dannenberg, J. J.; Zakrzewski, V. G.; Dapprich, S.; Daniels, A. D.; Strain, M. C.; Farkas, O.; Malick, D. K.; Rabuck, A. D.; Raghavachari, K.; Foresman, J. B.; Ortiz, J. V.; Cui, Q.; Baboul, A. G.; Clifford, S.; Cioslowski, J.; Stefanov, B. B.; Liu, G.; Liashenko, A.; Piskorz, P.; Komaromi, I.; Martin, R. L.; Fox, D. J.; Keith, T.; Al-Laham, M. A.; Peng, C. Y.; Nanayakkara, A.; Challacombe, M.; Gill, P. M. W.; Johnson, B.; Chen, W.; Wong, M. W.; Gonzalez, C.; Pople, J. A. *Gaussian 03*, revision C.02; Gaussian, Inc.: Wallingford, CT, 2004.
- (36) Yang, M.; Thompson, D. W.; Meyer, G. J. *Inorg. Chem.* **2000**, *39*, 3738.
- (37) Herber, R. C.; Nan, G.; Potenza, J. A.; Schugar, H. J.; Bino, A. *Inorg. Chem.* **1989**, *28*, 938–942.
- (38) Gentil, L. A.; Navaza, A.; Olabe, J. A.; Rigotti, G. E. *Inorg. Chim. Acta* **1991**, *179*, 89–96.
- (39) Evju, J. K.; Mann, K. R. *Chem. Mater.* **1999**, *11*, 1425–1433.
- (40) Gutmann, V. *Coord. Chem. Rev.* **1976**, *18*, 225–255.
- (41) (a) Lippert, E. Z. *Electrochemistry* **1957**, *61*, 962. (b) Lippert, E. Z. *Phys. Chem.* **1956**, *6*, 125. (c) Mataga, N.; Kaifu, Y.; Koizumi, M. *Bull. Chem. Soc. Jpn.* **1955**, *28*, 690. (d) Mataga, N.; Kaifu, Y.; Koizumi, M. *Bull. Chem. Soc. Jpn.* **1956**, *29*, 465.
- (42) Maruyama, M.; Matsuzawa, H.; Kaizu, Y. *Inorg. Chem.* **1995**, *34*, 3232–3240.